Chapter 5

Glycopolymer Induced Neuro-differentiation of Human Mesenchymal Stem Cells

5.1 Introduction

In the last several decades, a range of materials, consisting of metals, composites and ceramics, have been developed and used to improve the cell response on the material surface having micro/nano-topography and polymeric scaffolds at in-vitro and in-vivo conditions [209-212]. Metals are most preferred choice of materials due to their mechanical stability for implants, however, often the surfaces of these metal implants require surface modification for obtaining desirable physicochemical functionalities in order to improve their biological performance [213-215]. Despite all these modifications, there is still demand to find appropriate surface conditions to minimize the chance of breaking these implants at in-vivo conditions in the complex nature of the surrounding environment and tissues [216]. Thus, it is desirable to have materials with bioactive functions which can initiate the proliferation of the bone cells for bone regeneration at the targeted place and are degradable in the course of time. Thus the role of bio-based polymers, such as polysaccharide derivatives [217-219], polylactic acid [220,221], and polyhydroxyalkanoate [222,223] had increased in designing different architectures for applications in biological sciences [224-228].

The synthesis of homo and di-block glycopolymers, having relatively different types of hydrophilic characteristics, has also been explored for biomedical applications. Previously using the reversible addition−fragmentation chain-transfer (RAFT) process for synthesizing homo-glycopolymers and introducing PEG into the backbone was also reported for a wide range of applications. Similarly, the addition of aromatic rings in bio-based polymers had also examined for their role in modulating biocompatibility, thermal stability, and strength [229-

232]. Despite the potential of these bio-based polymers for their wide range of tunability in functional, structural, and variable architectures, their uses in biomedical applications have been relatively less explored compared to optical, electronic, and robotics applications. In recent years, researchers have demonstrated successful use of these for making biomaterials for improved cellular response and using them as a new choice of materials for cell differentiation [232-236].

In recent years enormous work has been done to develop materials having micro/nano-surface topography or metal nanoparticles (20-100 nm in size) has been tested for in-vivo and in-vitro biocompatibility [216-219]. The use of polymeric scaffolds at *in-vitro* and *in-vivo* conditions has also attracted great interest in providing 3D structural or functional support to cells in tissue engineering applications. Among the possible use of various materials, glycans may have several advantages due to their functional activities similar to natural systems [237]. Additionally, glycans can regulate cellular functions due to their flexibility for spatial distribution in the organization of glyco moieties and functional multivalent nature of glycoconjugates [238,239]. In this context, several biocompatible substrates with different surface chemical parameters were surveyed to investigate their role in stem cell differentiation [240,241]. In the past, various strategies were adopted to address the possibility of using stem cells (SCs) capable of neurogenic differentiation or supporting the regeneration of the nervous system [242-244]. This has gained usefulness in stem cell-assisted treatment, particularly enabling neural tissue regeneration by providing sufficient cell density in the region of vanished cells. Thus, the methods and processes which allow the retention of differentiated SCs functionality towards neurogenic lineage and strategies that can be employable in transplantation of these are a promising hope in treating various central nervous system (CNS) associated diseases. In the past, the emphasis has been on the origin and type of the

SCs that are decisive in their therapeutic usefulness. Neuronal SCs were obtained through direct isolation from the brain tissue [245,246] or differentiation of pluripotent stem cells [247,248]. Obtaining stem cells of embryonic or fetal origin has always been challenging due to source availability and ethical issues for therapeutic uses [249-255].

Recent studies also showed the possibility of differentiation of different types of mesenchymal stem cells (MSCs) into neuronal SCs, which may overcome the limitation of stem cells of embryonic or fetal origin [256,257]. The unique characteristic of multipotent MSCs is their plasticity and the capability to differentiate toward endodermal and ectodermal lineage cells [257-259]. Thus, several studies show that the SCs directed towards neural lineage showed greater potential for differentiating to functional neurons [252]. The objective of using stem cells in the context of CNS diseases therapy, the high neurogenic potential of MSCs gained significant attention to work on the processes that differentiate towards neural stem cells (NSCs) and neural progenitor cells (NPCs) [260,261]. Thus, multiple approaches were used to achieve neural differentiation of MSCs [262-264]. These strategies have shown limitations of the procedure, which are either time-consuming or end up with a relatively low proportion of NSCs while containing various cell types as well [265]. Whereas, the other methods that employ a monolayer culture of MSCs need to use several factors, namely, epidermal growth factor, supplements, nerve growth factor, retinoic acid, and resveratrol which have led to neural induction; however, the efficiency of these protocols is variable and their clinical usability is still limited [261]. The molecules with amino functionalities with groups containing thiol also induced neurogenic differentiation in stem cells [266,267].

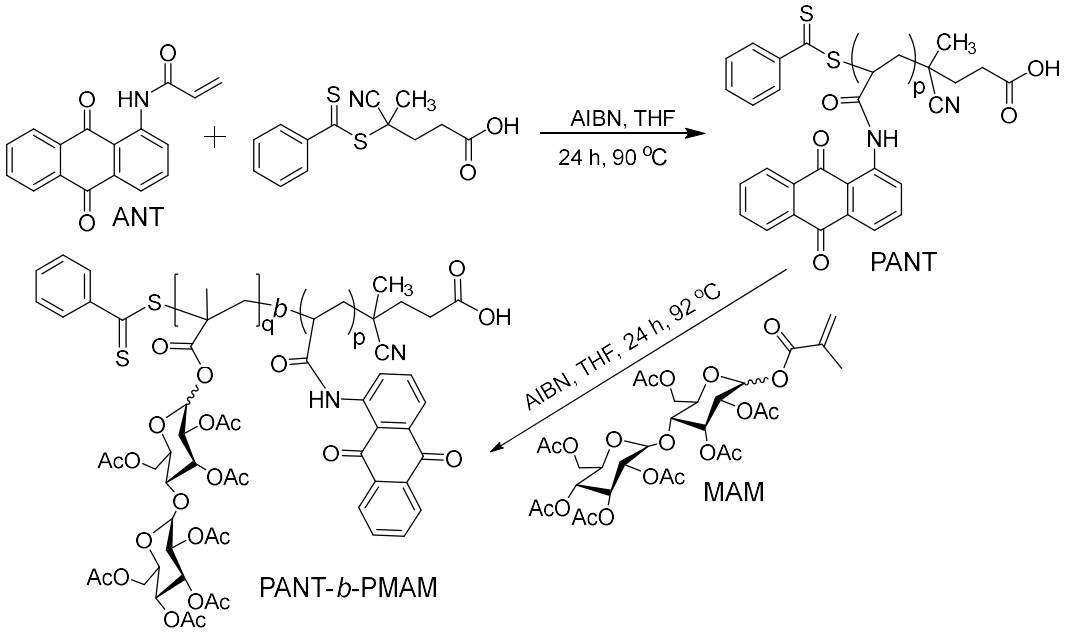

Figure 5.1: RAFT polymerization of (1) P(ANT), (2) P(ANT-b-PMAM) and ATRP polymerization is (3) P(PMAM).

The cellular response to biomaterials is mainly influenced by hydrophilicity, chemical functionality, structural variations, and surface morphologies, which enables tunable cell-surface interaction [268,269]. The polar characteristics of biomolecules used to prepare surfaces for better cell adhesion and viability mainly demonstrate comfortable support for cell attachment and advocate undisturbed proliferation [270-272]. Whereas, the use of non-polar characteristics of molecules used for preparing surfaces for making them suitable for cell studies is relatively less explored [273]. The superiority of hydrophobic surfaces has been demonstrated for enhanced differentiation of embryonic stem cell-derived embryoid bodies [240]. Therefore, investigating the role of materials having both polar and non-polar characteristics in controlling cellular response may provide a better understanding of cell-material interaction. Previously the effect of glycopolymers having various pendant spacer lengths of glucose moiety for cell adhesion, viability, and proliferation was investigated [274].

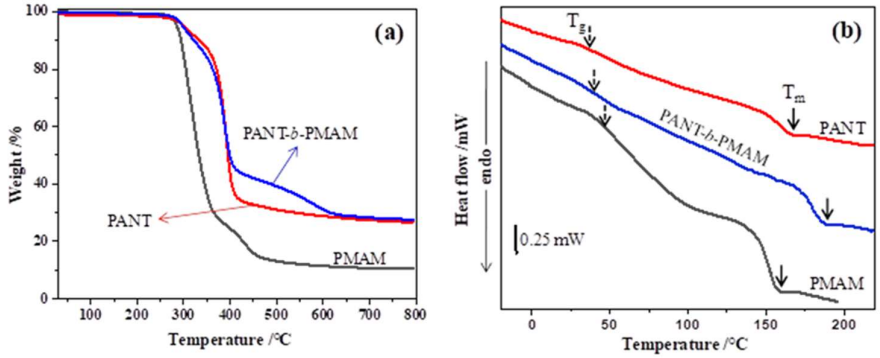

*Figure 5.2: Synthesized polymers (**a**) TGA curves and (**b**) DSC thermograms on 2nd heating under nitrogen atmosphere.*

Further, the addition of poly(ethylene oxide) with glycopolymers was also used to study their biocompatibility [231,272]. In the past, different architectures were designed from anthraquinone functional moiety containing eco-friendly polymer for different applications [261-265]. This study describes glycopolymers synthesized with either polar (maltose), non-polar (aminoanthraquinone), or both for hMSC differentiation capability.

5.2 Glycopolymers preparation and characterization

The synthesis of glycopolymers were done by the Dr AVS Sainath from CSIR-IICT, Hyderabad were the PANT and di-block copolymer, PANT-*b*-PMAM were synthesized from ANT (chemical structure confirmation given in Figures A2 and A3 of Annexure II), PANT-macroinitiator and MAM (Figures A5 and A6 in Annexure II) using the RAFT process as presented in **Figure 5.1**. The detail of the synthesis and characterisation are provided Annexure 1. The PANT, PANT-*b*-PMAM, and PMAM polymers' TGA and DSC curves are presented in **Figure 5.2(a, b)**. The 5% ($T_{d5\%}$) and 10% ($T_{d10\%}$) degradation temperatures, % char at 750 °C and thermal transitions such as glass- (T_g) and melt-transition (T_m) temperature values are tabulated in Table A2 of annexure II.

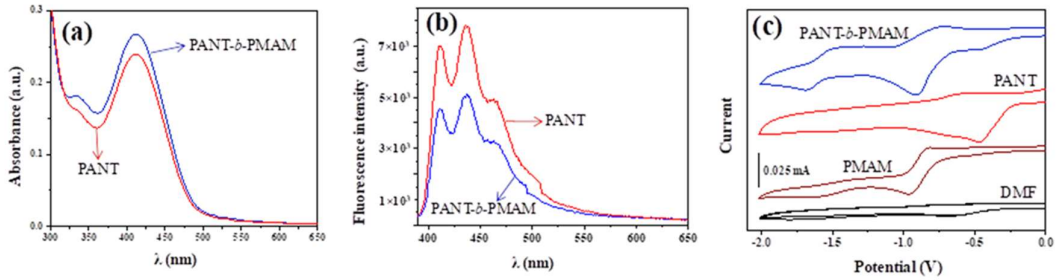

*Figure 5.3: (a) UV-Vis spectra of PANT and PANT-b-PMAM, (**b**) Fluorescence spectra of PANT and PANT-b-PMAM (c) Cyclic voltagram (CV) response of synthesized polymers.*

These results indicate that the synthesized polymers are semi-crystalline in nature and further, the DSC studies of these polymers were supporting the XRD data, by exhibiting endothermic melt transition temperatures of the polymers. UV-vis spectra of the PANT and PANT-*b*-PMAM were measured in dimethyl sulfoxide (DMSO) solution (1×10^{-6} M). The absorption spectrum of the PANT (**Figure 5.3a**) showed a broad absorption peak at 410 nm (λ_{max}) due to π-π* transition of polymer chain pendant anthraquinone moieties and its aggregations. The PANT-*b*-PMHAM solution exhibited a peak at 412 nm due to π-π* transition of PANT segment pendant anthraquinone moieties and its aggregations and a shoulder peak appeared at 335 nm. On the other hand, the absorption spectrum of the ANT showed a broad absorption peak at 409 nm (λ_{max}) due to the π-π* transition of anthraquinone and its aggregations [266]. Fluorescence spectra of the PANT and PANT-*b*-PMAM were measured in DMSO solution (1×10^{-6} M) and are presented in **Figure 5.3b**. The PANT and PANT-*b*-PMAM polymer solutions excitations were accomplished at 379 nm. The PANT exhibited a broad emission peak at 436 nm along with a peak at 411 nm due to π*-π transition. Similarly, PANT-*b*-PMAM showed a broad emission peak at 438 nm along with a peak at 412 nm due to π*-π transition. The ANT solution excitation was accomplished at 379 nm. The ANT showed a broad emission peak at 438 nm along with a peak at 413 nm due to π*-π transition [267].

Cyclic voltammograms of the PANT and PANT-*b*-PMHAM polymers at 10 mM in DMF using a supporting electrolyte, 0.1 M tetra-*n*-butyl-ammonium hexafluoro-phosphate at 100 mV s^{-1} scan rate are presented in **Figure 5.3c**. The PANT exhibited one-state reduction at -0.46 V, whereas the PANT-*b*-PMHAM polymer showed two-state reductions at -0.91 V, and -1.6 V. The ANT monomer exhibited three redox potential peaks [268] at -0.71, -1.05 and -1.47 V.

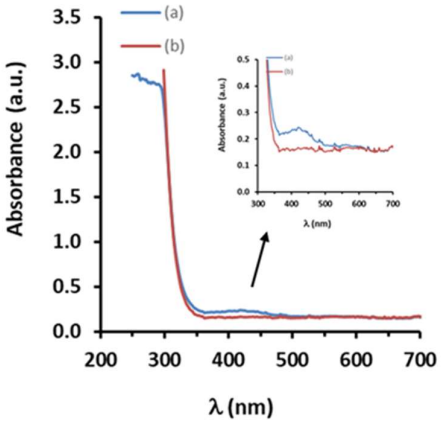

Figure 5.4: UV-Vis spectra of PANT and P(ANT-b-PMAM) thin films.

The PMAM, PANT, and PANT-*b*-PMAM were separately dissolved in a diluted DMSO, and respective films were deposited on clean glass slides by spin coating. UV-Vis spectra of PANT and PANT-*b*-PMAM film showed a noticeable broad peak at λ_{max}= 412 nm (**Figure 5.4**). This peak position precisely coincides with the absorption peak of corresponding glycopolymers obtained in their solution form. The synthesized glycopolymers were of three distinct characteristics, polar, which readily dissolves in water (PMAM); non-polar, which dissolves in a non-aqueous solvent (PANT); and PANT-*b*-PMAM, which has both types of functional moieties. Thus, the variation of the proportion in functional moieties of the coatings determines their polar surface characteristics, enabling us to study their role in the adhesion, proliferation, and differentiation of hMSCs.

Field emission scanning electron microscopy (FE-SEM) image of PMAM showed a smooth film surface without any specific morphologies (**Figure 5.5a),** whereas PANT demonstrates the uniform distribution of ~ 100 nm diameter spherical shape granules with distinct boundaries (**Figure 5.5b**). This attributes to the self-assembly of non-polar moieties in glycopolymer material during film formation at the surface. The di-block glycopolymer (PANT-*b*-PMAM) coating surface morphology showed a representation of

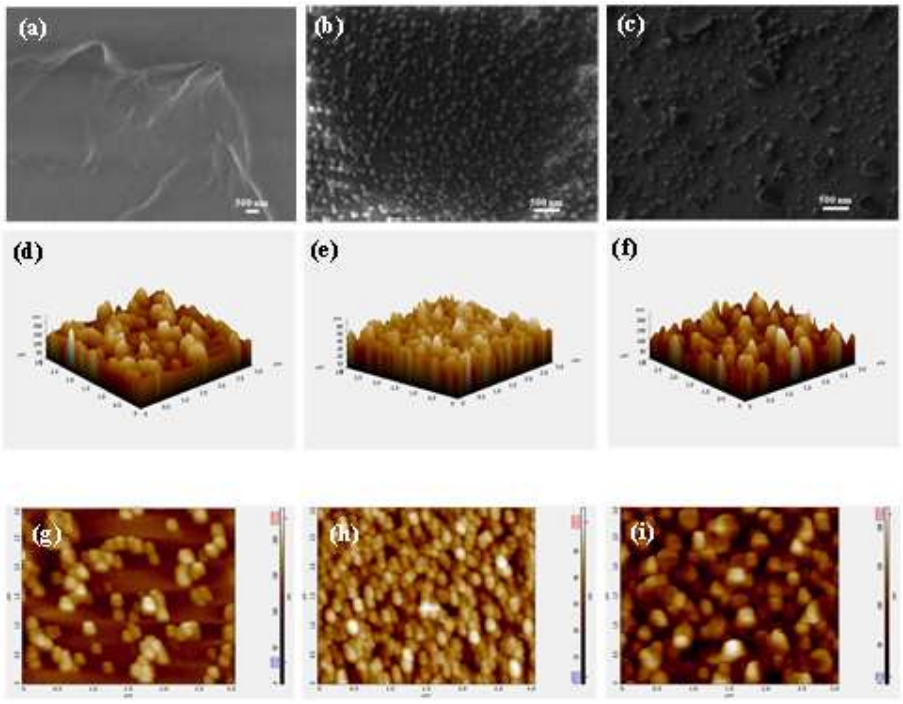

*Figure 5.5: FE-SEM images of (**a**) PMAM, (**b**) PANT and (**c**) P(ANT-b-PMAM). 3D and 2D AFM images of (d&g) PMAM, (e&h) PANT and (f&i) P(ANT-b-PMAM).*

mixed-sized granules with a relatively lesser density (**Figure 5.5c**) as compared to that observed at the PANT film surface. AFM analysis of these film surfaces was performed to examine surface morphology, and the results are shown in **Figure 5.5(d-i)**. AFM images in **Figure 5.5e&h** demonstrated a tightly packed assembly of polymeric units with distinct boundaries, leading to nano-assemblies of the PANT glycopolymer with a height in the range

of 50 nm to 100 nm. PMAM surface showed a relatively less packed distribution of localized nano-assemblies. The di-block copolymer surface topological view is quite similar in the packing distribution of the nano-assemblies of the PANT polymeric material; however, the height of nano granules increased in the range of 50 nm to 200 nm. The results clearly indicated the formation of localized nano-assemblies of glycopolymers and their distribution. The results showed a correlation between the increase in the size of nano-assemblies and a decrease in packing density with their elevated non-polar characteristics.

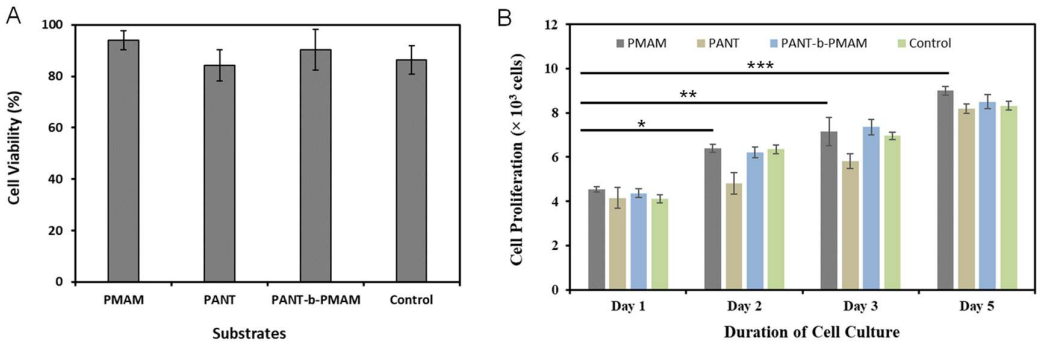

Figure 5.6: (A) Cell viability of hMSCs seeded on thin films of PMAM, PANT, P(ANT-b-PMAM) and tissue culture plastic surface (TCP) (control) was measured by MTT assay at 24 h. The data represents with n = 27 coated surface and 9 control conditions, (B) Cell proliferation of hMSC cells seeded on different chips along with control was checked for different days. The data represents with n = 9 coated surface for each polymer and control conditions for each day.

5.3 Viability and proliferation of hMSCs on glycopolymer surfaces

The hMSCs response was studied with glycopolymers having polar and non-polar characteristics and representing simultaneous architectures of both traits in the glycopolymer units in directing their differentiation while maintaining desired adhesion and viable characteristics. hMSCs were seeded on these three different types of surfaces prepared by spin

coating of glycopolymers and cell viability and proliferation were examined by MTT assay (**Figure 5.6A-B**).

Cell viability on PMAM coated surface was relatively higher than PANT and P(ANT-*b*-PMAM). The cell viability on di-block polymer, which contains both functional moieties, was better than PANT and slightly compromised in response to PMAM. Further to confirm the cell viability, microscopic analysis was performed using Hoechst 33342/PI dual staining after 24 h of cell seeding on these glycopolymer-coated surfaces and compared with the control condition (**Figure 5.7**). Microscopic images of dual-stained Hoechst 33342/PI along with phase-contrast images of cells on all polymeric substrates clearly showed that cells are viable as no red-stained cells, an indication of the non-viable cell population. These results are very similar to the observations obtained from the MTT assay. The hMSCs proliferation results on these polymeric coating surfaces showed a gradual increase in the cell number from day 1 to day 7 (**Figure 5.4B**). This indicates that the viable cells on these surfaces further participate in proliferation.

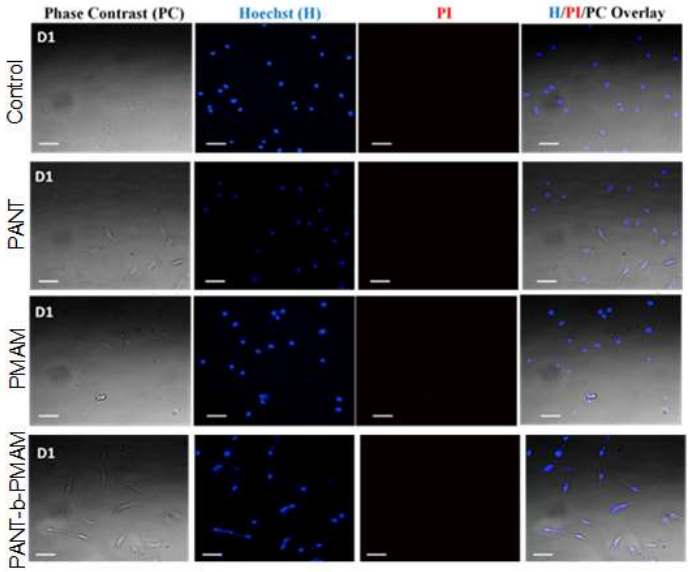

Figure 5.7: Hoechst 33342/PI dual staining of cells seeded on TCP (control), PMAM, PANT and P(ANT-b-PMAM).

5.4 Neurogenic Differentiation of hMSCs on glycopolymer surfaces

Previously, the superiority of hydrophobic surfaces with amino functionalities along with sulfur-containing groups was demonstrated for neurogenic differentiation of stem cells [58,59]. The glycopolymers synthesized here with different architectures were incorporated with unique characteristics of variable polar characteristics and amine and sulfur groups in their subunits. The effect of these glycopolymers on their capability

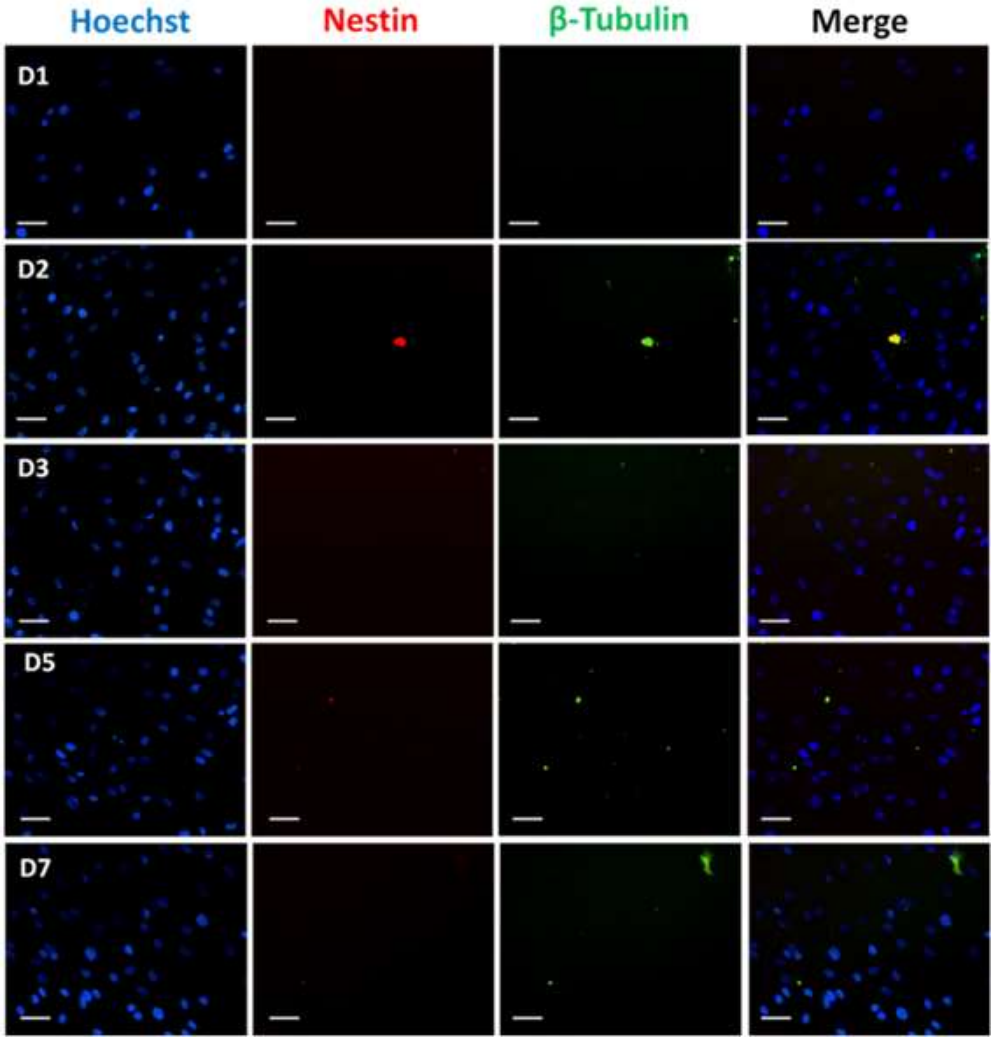

Figure 5.8: Quantification of cell surface markers nestin (red) and β-tubulin (green) for cells seeded on control (tissue culture plastic surface) by immunocytochemistry. DAPI was used as counter stain for identifying the cellular nuclei (blue). Scale bar: 100 µm.

towards initiating neurodifferentiation was characterized by staining hMSCs grown on these surfaces on different days by immunostaining with neuronal-specific markers, Nestin, β tubulin-III, and GFAP antibodies (**Figure 5.8** for control, **Figure 5.9** for PMAM, **Figure 5.10** for PANT and **Figure 5.11** for P(ANT-b-PMAM)). The experimental details are described in Annexure I. Nestin is a marker for neural stem cells which can further differentiate into neurons, astrocytes, and oligodendrocytes expressing β tubulin-III , GFAP and O4 markers, respectively [49,67].

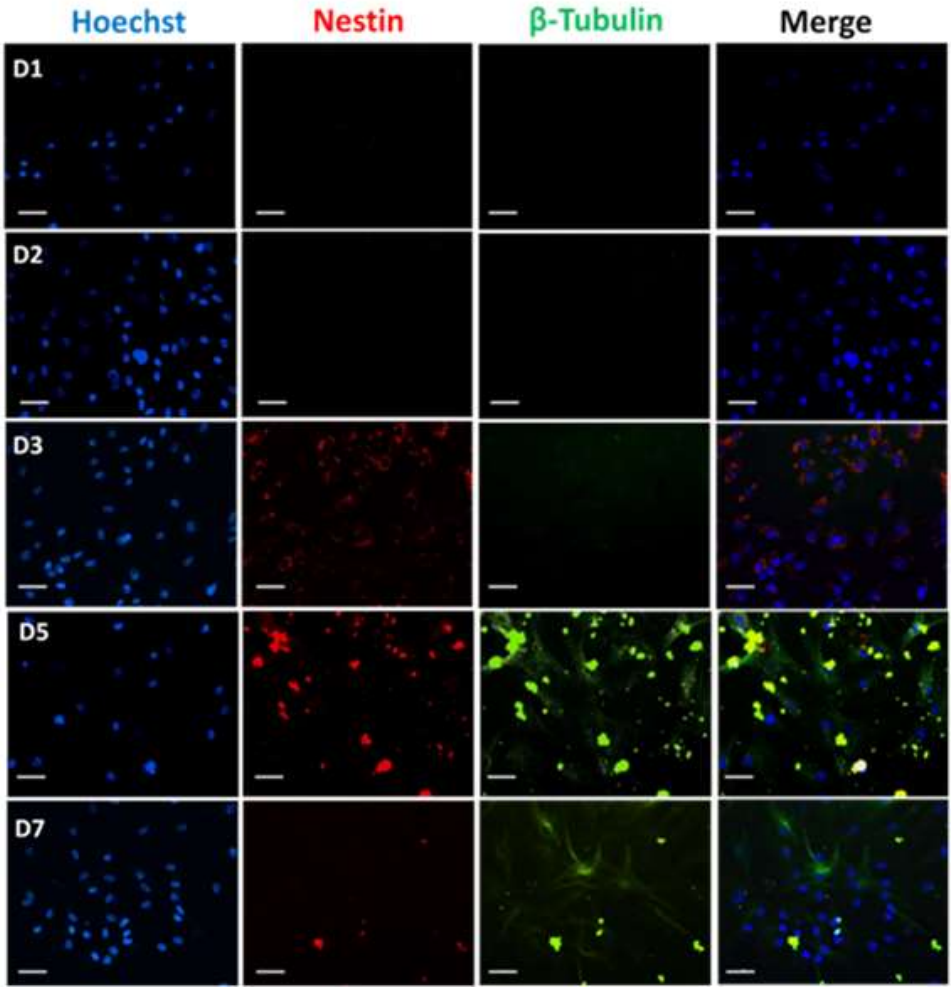

Figure 5.9: Quantification of cell surface markers of nestin (red) and β-tubulin (green) for cells seeded on PMAM surface by immunocytochemistry. DAPI was used as counter stain for identifying the cellular nuclei (blue). Scale bar: 100 μm.

The expression of nestin was seen earliest for di-block polymer on day 2 as seen in (**Figure 5.11**) compared to PANT (**Figure 5.9**) and PMAM (**Figure 5.10**). This result indicated that the presence of functional moieties of both natures, polar and non-polar ameliorates the early neurodifferentiation process. As time progressed, the seeded cells showed a green colour signal expressing β tubulin-III attributing maturation of differentiated MSC towards neurons. These expressions were absent in the control

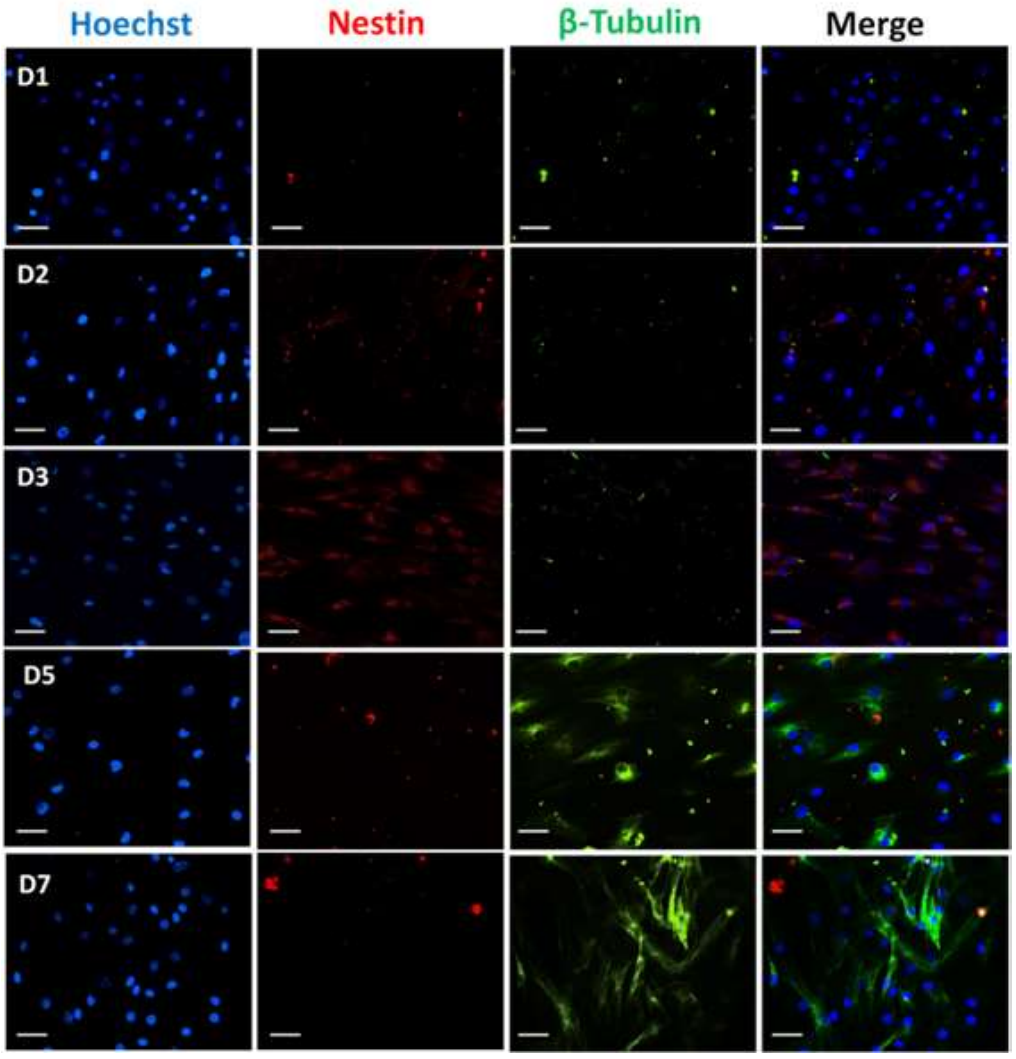

Figure 5.10: Quantification of cell surface markers of nestin (red) and β-tubulin (green) for cells seeded on PANT surface by immunocytochemistry. DAPI was used as counter stain for identifying the cellular nuclei (blue). Scale bar: 100 µm.

condition (**Figure 5.8**). These expressions were found highest in the hMSCs seeded on thin films of di-block polymer (**Figure 5.11**). The cells were found to be elongated with time, resembling the shape of neurons. No expression of GFAP antibodies was found in the differentiated cells.

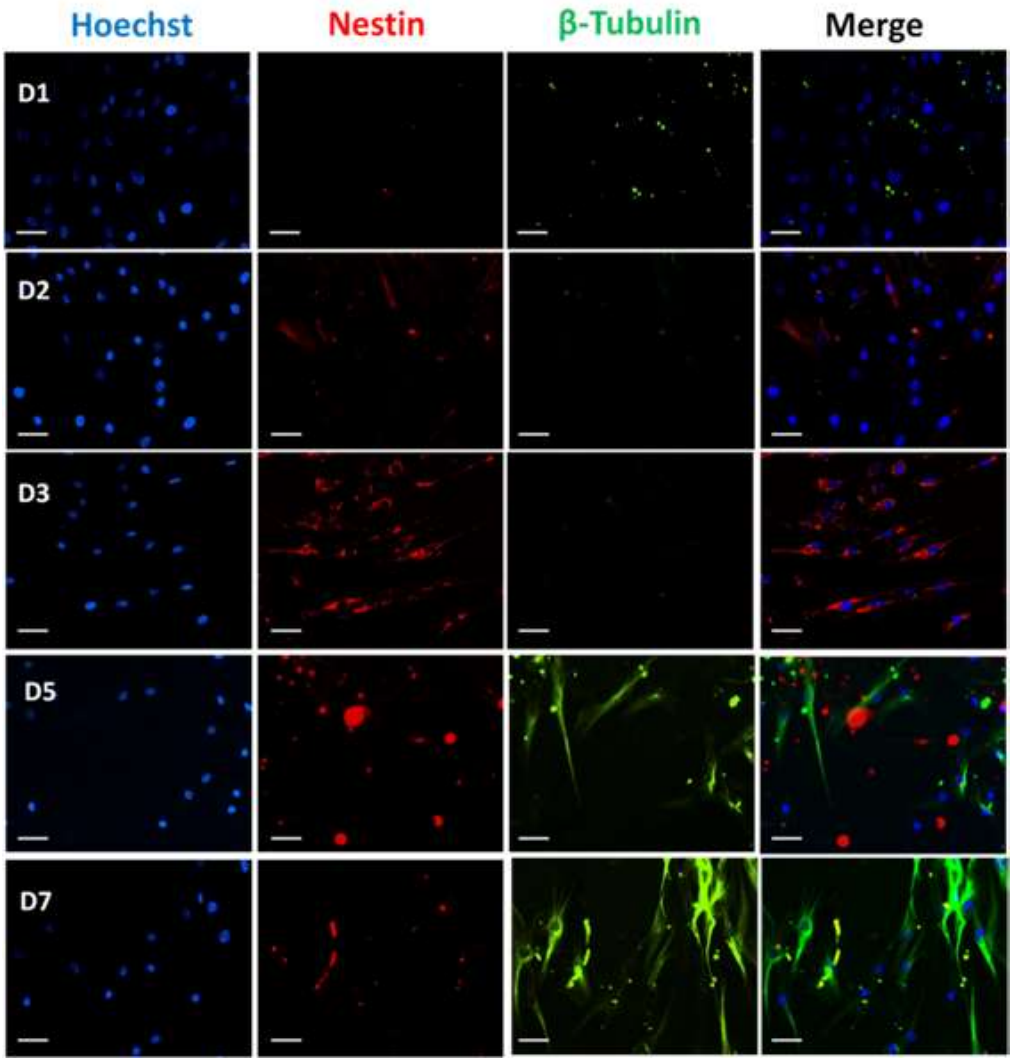

Figure 5.11: Quantification of cell surface markers of nestin (red) and β-tubulin (green) for cells seeded on P(ANT-b-PMAM) surface by immunocytochemistry. DAPI was used as counter stain for identifying the cellular nuclei (blue). Scale bar: 100 µm.

5.5 Mitochondrial membrane potential (MMP) quantification

JC-1, a potentiometric dye, was used to evaluate the changes occurring in mitochondrial membrane potential (MMP) during the differentiation process of hMSCs. JC-1 dye accumulates in mitochondria depending on its membrane potential and exhibits different fluorescence characteristics [270].

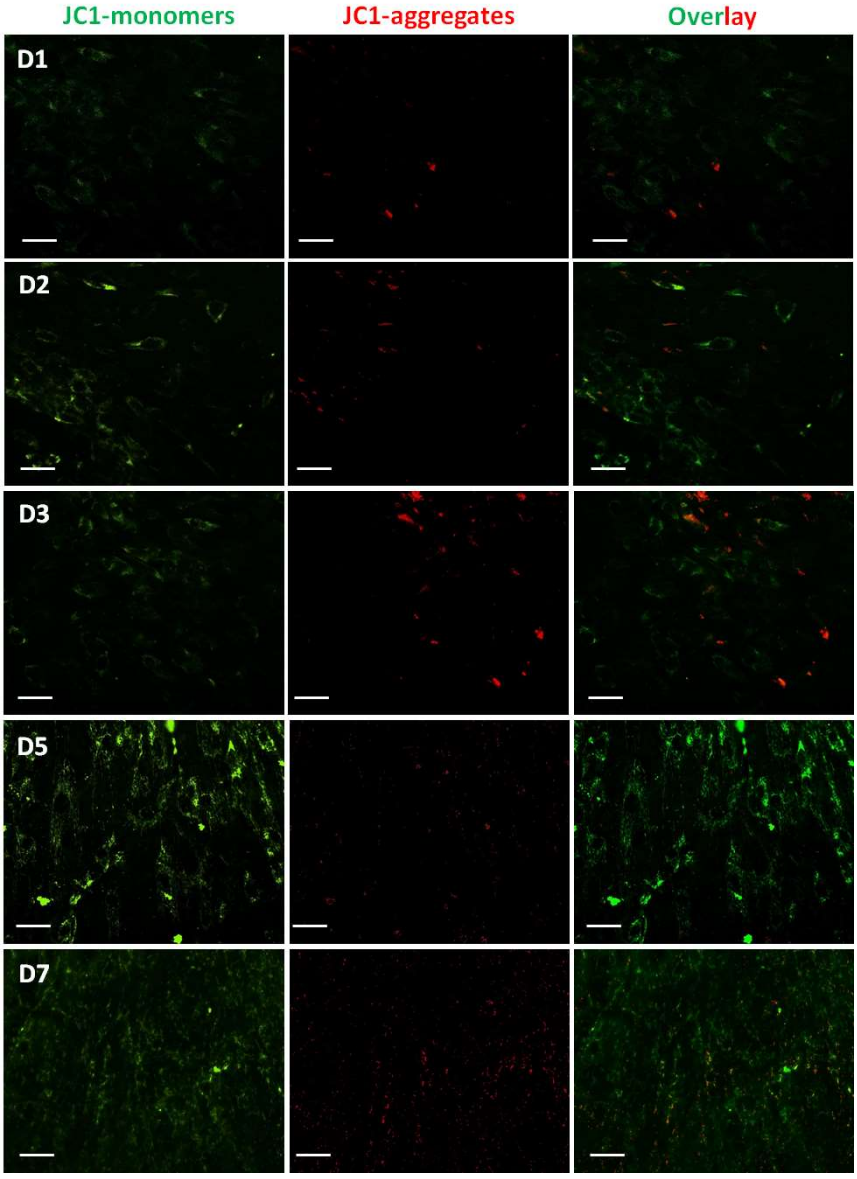

Figure 5.12: Assessment of mitochondrial membrane potential of cells seeded on control condition for day 1 (D1), day 2 (D2), day 3 (D3) day 5 (D5) and day 7 (D7) of culture. Scale bar: 100 µm.

Depolarized mitochondria with low MMP (less negative) fail to sequester JC-1 and result in the formation of monomers that fluoresce green. The details about the experiment procedure for JC-1 dye is described in Annexure I.

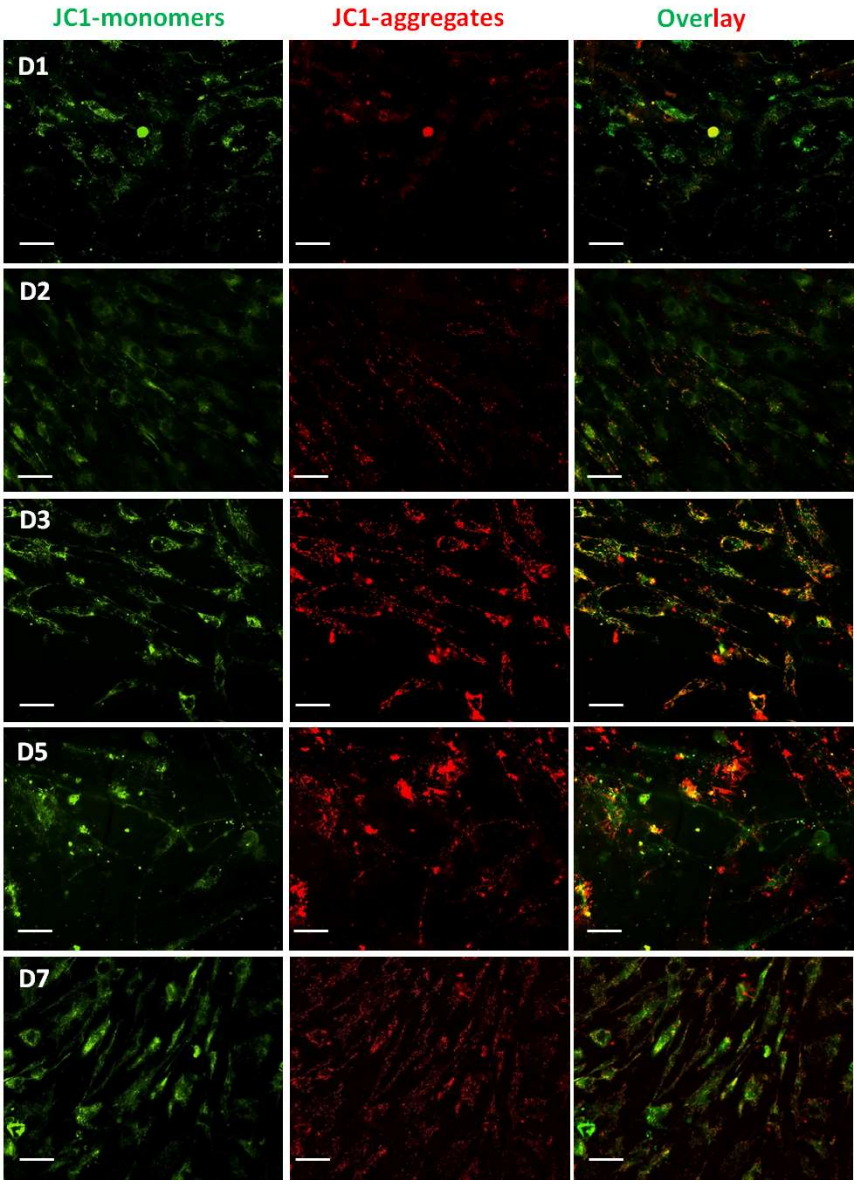

Figure 5.13: Assessment of mitochondrial membrane potential of cells seeded on PMAM surface for day 1 (D1), day 2 (D2), day 3 (D3) day 5 (D5) and day 7 (D7) of culture. Scale bar: 100 µm.

In comparison, higher MMP forms JC-1 aggregates which yield red fluorescence. JC-1 staining was monitored on day 1, 2, 3, 5 and 7 for cells seeded on thin films of different polymeric molecules compared to control cells (**Figure 5.12** for control, **Figure 5.13** for PMAM, **Figure 5.14** for PANT and **Figure 5.15** for P(ANT-b-PMAM)).

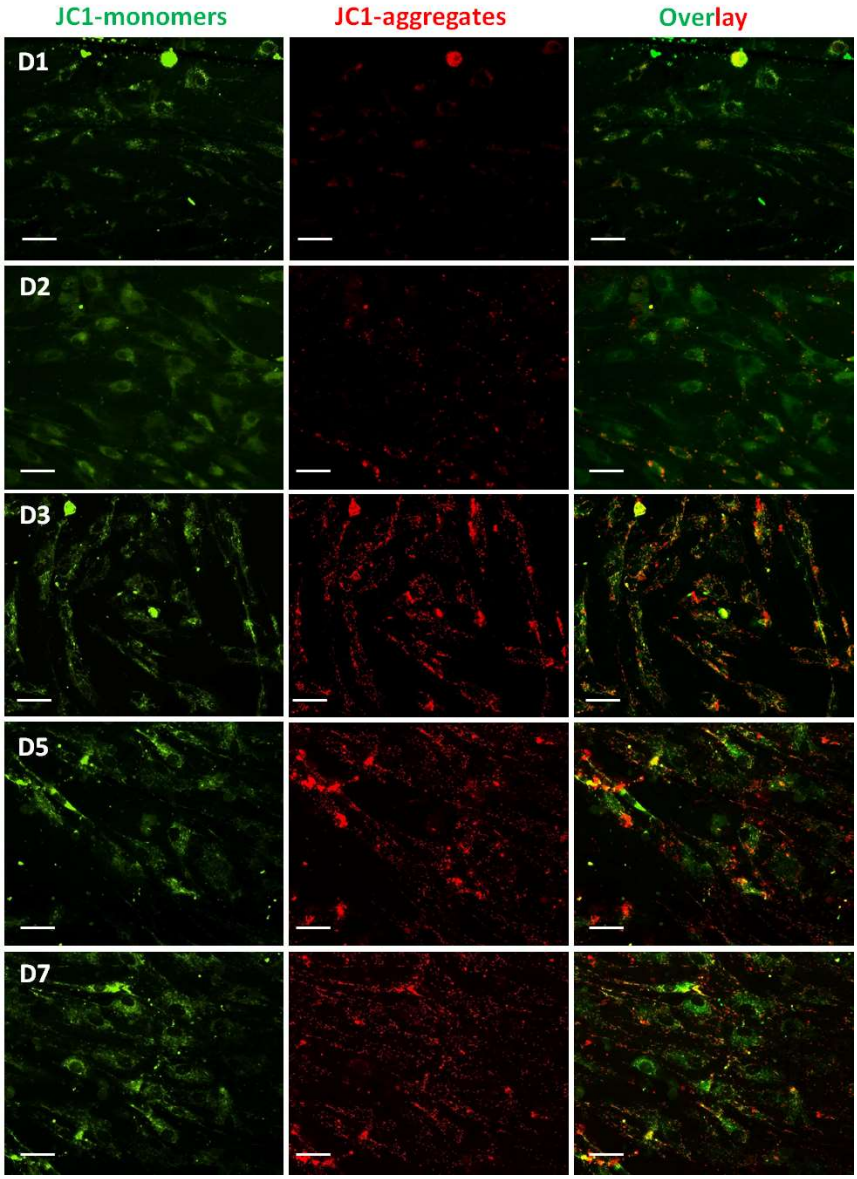

Figure 5.14: Assessment of mitochondrial membrane potential of cells seeded on PANT surface for day 1 (D1), day 2 (D2), day 3 (D3) day 5 (D5) and day 7 (D7) of culture. Scale bar: 100 µm.

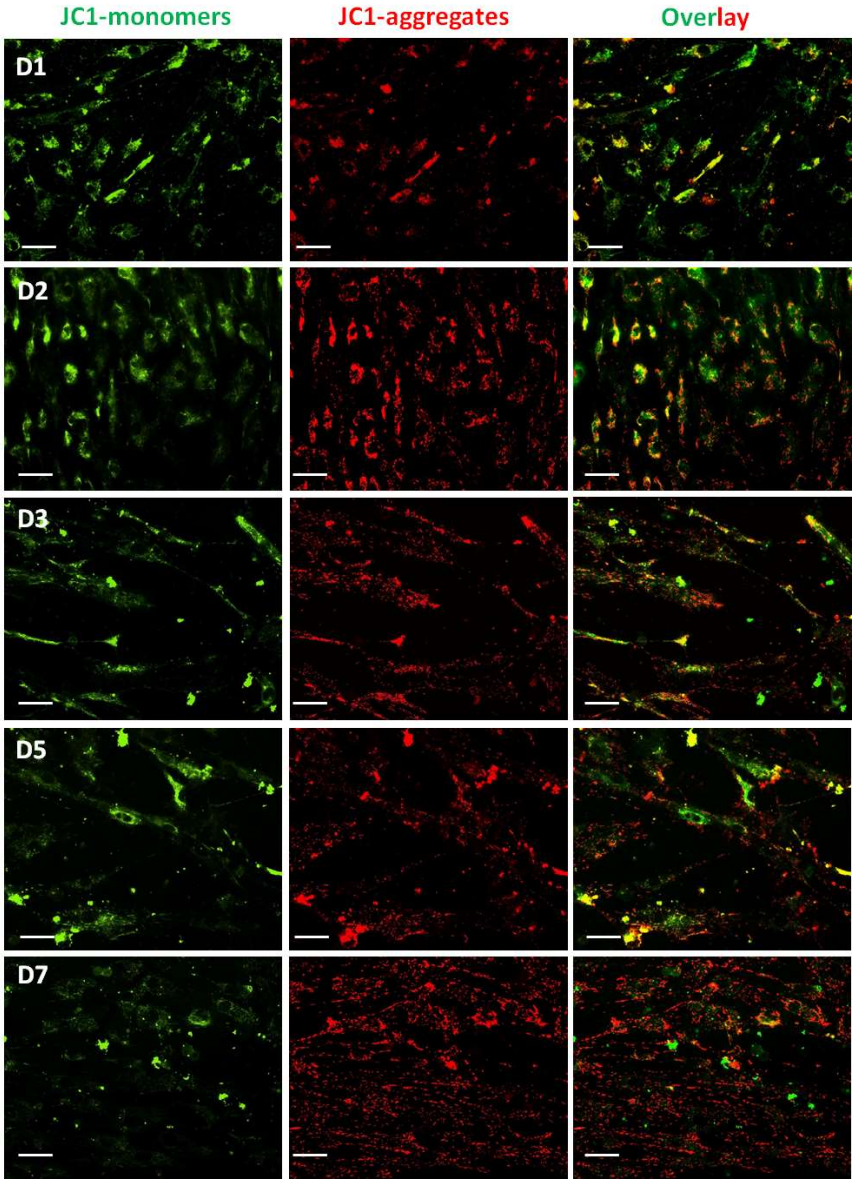

Figure 5.15: Assessment of mitochondrial membrane potential of cells seeded on P(ANT-b-PMAM) surface for day 1 (D1), day 2 (D2), day 3 (D3) day 5 (D5) and day 7 (D7) of culture. Scale bar: 100 µm.

This provides information about the role of the energy center, mitochondria, during the differentiation process as it is expected to show an elevated expression in neuronal cells due to their relatively high metabolic rates compared to undifferentiated hMSCs [275]. On day 1, cells seeded on di-block polymer molecules emitted red color while those seeded on the other

two polymeric molecules yielded a green signal, as shown in (**Figure 5.15**). This indicated that the mitochondria of the differentiated cells are metabolically more active and thereby expressing high MMP. As the day progressed, an increase in red/green fluorescence expressing high MMP. As the day progressed, an increase in red/green fluorescence intensity ratio was observed, attributing to elevation in MMP. On day 7, the high red intensity was seen in differentiated hMSCs compared to control cells (**Figure 5.12**). This indicated mitochondrial function is crucial for stem cell fate decision and high MMP may act as a vital cellular factor to induce the neurodifferentiation process.

5.6 Intracellular ROS quantification

The intracellular ROS production was also examined using DCFH-DA dye in the cells at different days grown on three different types of glycopolymer coatings and compared with the control condition (**Figure 5.16**). DCFH-DA, a cell-permeant dye, is deacetylated to the non-fluorescent compound by cellular esterases and further oxidized to form a green fluorescent 2'-7'dichlorofluorescein (DCF) product in the presence of ROS. The onset of the green signal on day 2 for the cells seeded on di-block polymer indicated the initiation of differentiation of hMSCs as similar to that expression observed by neurogenic markers (**Figure 5.8** to **Figure 5.11**).

The green signal increases during the progression of the differentiation process at increased days of cell culture towards their neuronal lineage. This suggests that the changes in the level of intracellular ROS production during the stem differentiation process towards neurogenic lineages coincide with a neurogenic expression of a similar pattern on these glycopolymer coatings. Our observations are also in line with findings reported in the past, where it had demonstrated that an elevated level of ROS plays a vital role as an intracellular messenger in

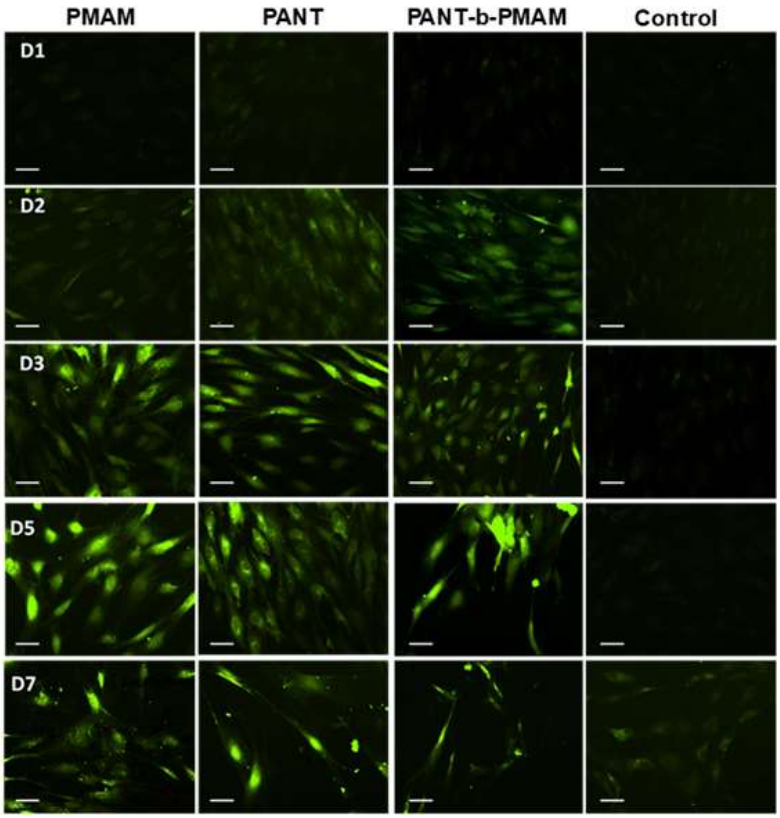

Figure 5.16: Time-dependent generations of ROS after day 1 (D1), day 2 (D2), day 3 (D3), day 5 (D5) and day 7 (D7) of seeding hMSCs on thin films of PMAM, PANT, P(ANT-b-PMAM) and control detected by measuring the fluorescence intensity using DCFH-DA dye. Scale bar: 100μm.

dictating the differentiation process and is tightly linked with MMP [68,69]. The surface prepared by the coating of glycopolymer P(ANT-*b*-PMAM) having maltose moiety with amine and thiol in the backbone of polymer demonstrated superiority in showing hyperpolarization of mitochondria membrane relatively much earlier than the expression elevated intracellular ROS production, which initiates differentiation of hMSCs into neuronal lineages. Our findings are inconsistent with previously reported studies where the role of amine and thiol has been demonstrated for the neurogenic differentiation of stem cells [276,277]. Thus, this finding highlights the early expression of MMP, which further elevate the ROS production for initiating the neurogenic differentiation process.